

## **Electro - copolymerization of symmetric flower-like Luminol - Aniline - Hollow TiO<sub>2</sub>-NH<sub>2</sub> nano-shell polymer in ionic liquid for Acetochlor detection**

*Hongying Cheng<sup>\*</sup>, Song Liu, Cuiying Hu, Hongxia Wang*

School of chemical biology and materials engineering, Suzhou University of Science and Technology, Suzhou, 215009, Jiangsu, China

\*E-mail: [chenghy1015@126.com](mailto:chenghy1015@126.com)

*Received: 8 January 2018 / Accepted: 2 March 2018 / Published: 10 April 2018*

A novel flower-like film composed of uniform hollow TiO<sub>2</sub>-NH<sub>2</sub> nano-shell (HTNs), luminol and aniline was synthesized by electro-copolymerization method in acidic ionic liquid EmimCl (IL, 1-ethyl-3-methylimidazolium chloride). The surficial morphology of the film was characterized by scanning electron microscope (SEM), transmission electron microscope (TEM), selected-area electron diffraction (SAED) and atomic force microscope (AFM), which showed the polycrystalline property. Its copolymerization mechanism was discussed in detail, which presented symmetric arrangement. The most obvious multiple increase of peak current in CV indicated the conjugate of HTNs in luminol structure and in aromatic ring skeleton. This film with excellent electrocatalysis performance used for nonelectroactive acetochlor (ACT) detection showed the lowest catalytic potential. Some important parameters were optimized for a homogeneous film and for a sensitive detection. On the optimum film, the electrocatalysis sensor exhibited a linear response within the concentration range of ACT from  $2.0 \times 10^{-7}$  M to  $1.5 \times 10^{-5}$  M, and an absolute detection limit of  $0.15 \times 10^{-9}$  M at a signal-to-noise ratio of 3. Then the proposed method was used for the detection of ACT residue in the real strawberry sample with good results. The promising sensor presents good reproducibility and stability, providing a new fast and sensitive method for the analysis of real samples in environment.

**Keywords:** Acetochlor; homogeneous nano-conjugation; Electrocatalysis; Ionic liquid EmimCl (1-ethyl-3-methylimidazolium chloride);

### **1. INTRODUCTION**

Acetochlor (ACT) has already been classified as a B-2 carcinogen by the U.S. Environmental Protection Agency (USEPA, 2000, 2006, 2007) [1]. However it has been still used widely in agricultural fields for control of grasses and broad leaf weeds [2, 3] resulted in pollution in the soil and

adjacent surface water. Moreover, some studies have reported that ACT is a latent endocrine disruptor [4] due to its genetic toxicity [5] and apoptosis [6]. So it is important to explore a stable, facile and sensitive method for the determination of the ACT residue in environment. As reported, some typical methods have been established such as the liquid chromatography-mass spectrometry (LC-MS) [7], ultra-HPLC-MS/MS [8], gas chromatography-mass spectrometry (GC-MS) [9] and GC with electron capture detection (GC-ECD) [10]. Because of the nonelectroactivity of ACT, some methods including the immunosorbent assays (IA) [11], piezoelectric Biosensor (PB) [12], fluorescence polarization immunoassay (FPI) [13], and photoelectrochemical biosensor (PEB) [14, 15] were used to indirectly detect ACT. Nevertheless, these methods need costly instruments and time-consuming preprocessing. Then, the convenient and quick method for ACT detection attracts the attention and interest of researchers.

Because of high catalytic activity and good electronic conductivity, the hollow  $\text{TiO}_2$  nano-shell (HTNs) which has also been successfully synthesized by regulating the shape, size, shell thickness and crystal phase has been used in many electro-fields such as electrochemistry [16], ECL intensifier [17], photoelectrocatalysis [18]. Also, the copolymer films of poly (luminol / aniline) (PLA) via the linkage of para-position amidogen and two phenyl rings were also performed on the electrode surface to promote charge transfer and to improve the chemical properties over the pure single poly-film [19]. Up to now, the synthesis methods for PLA included chemical oxidative polymerization [20] with the average diameter around 100 nm and electrochemical copolymerization on line [21] with the average diameter only around 30 nm. In fact, the connection pattern in the polymer by the chemical polymerization were enwrapped and hybridized to form the uniform copolymers. The arrangement of the molecules was impossible to observe clearly, but only through the copolymerization mechanism. Inspired by this, when  $\text{TiO}_2$  nano-shell with luminol and aniline copolymerized at the same time, what shape, configuration or the arrangement of copolymer will be?

In this work, the HTNs were synthesized with a  $\text{SiO}_2$ -sacrificial approach. After being grafted with  $-\text{NH}_2$ , HTNs- $\text{NH}_2$  with luminol and aniline were electro polymerized at the same time on the surface of indium tin oxide (ITO). In order to improve the ionic conductivity, biocompatibility and molecular viscosity, ionic liquid (IL) was also previously added into the mixture. Considering the different electron transport capability of HTNs, the dosages of luminol and aniline, and the scanning rate were optimized in the process of copolymerization to avoid the slice of polymer and form the homogeneous film. The morphology of the copolymer film was characterized by instrument. The ordered symmetric arrangement of HTNs in the electro co-polymerization and the structure of the film were discussed too, which formed a flower-like structure to maintain the symmetrical structure. After optimization of the electro copolymerization parameters and detection conditions, the copolymer electrode showed the excellent electrocatalytic performance.

Although there is no electrochemical active group in ACT structure, the extra electrochemical signal presented a linear relationship to the concentration of ACT on this proposed sensor after scanning 5 cycles in the 0.5 M  $\text{H}_2\text{SO}_4$ . The electrocatalysis mechanism of ACT on it was analyzed to be the process of hydrolysis and catalytic oxidation, so the detection of ACT was considered to be a two-step electrocatalytic mode. And the result was credible and remarkable.

## 2. EXPERIMENTAL

### 2.1. Materials and reagents

Nano-TiO<sub>2</sub> powder (P-25) was purchased from Degussa Corporation (USA, 70% in anatase phase and 30% in rutile phase, 30–50 nm in diameter). Luminol and aniline were obtained from Fluka Chemical Co. (USA). (3-Aminopropyl) Triethoxysilane (APTES, 99%) was obtained from Aladdin Chemical Co. Tetrabutyl titanate (TBOT, 98%), tetraethyl orthosilicate (TEOS, 99%) and all of the other chemicals were obtained from Sinopharm Chemical Reagent Co. Shanghai (China). They were of analytical grade and were used without further purification. Phosphate buffer solutions (0.2 M) were prepared by varying the ratio of NaH<sub>2</sub>PO<sub>4</sub> to Na<sub>2</sub>HPO<sub>4</sub> and NaOH. The indium tin oxide (ITO) glass was purchased from Suzhou Nippon Sheet Glass Electronics Co. Ltd. (Suzhou, China). Ultra pure water was prepared with an ALH-6000-U ultra pure water system (Aquapro, China) and was used throughout the experiments. SPE columns (PSA, 500 mg, 3 mL) purchased from Agela Technologies (China) were used in solid phase microextraction (SPME).

### 2.2. Apparatus and instruments

Cyclic voltammetry (CV), electrochemical impedance spectroscopy (EIS) and differential pulse voltammetry (DPV, with scan rate 100 mV/s) measurements were performed on a CHI660B electrochemical workstation (Chenhua Instruments Co. Ltd, Shanghai, P.R. China). A conventional three electrode cell set-up was comprised of platinum wire, a saturated calomel reference electrode (SCE) and modified electrocatalysis sensor as counter, reference and working electrodes, respectively. The surface of ITO was degreased with acetone, rinsed with distilled water and used as the bare electrode. The area of ITO was maintained constant as 1 cm<sup>2</sup> by masking the rest of the electrode with lacquer. Fourier transform infrared (FTIR, Avatar 360, German) was used to characterize the grafted group on the surface of HTNs. A SEM (S-4700, Hitachi, Japan), a TEM (FEL, USA), a SEAD and an AFM were used to observe the size and morphology of the nanomaterials. An Allegra 64R Centrifuge (Beckman Coulter, USA) was used to isolate the nanomaterials from the mother liquid.

### 2.3. Synthesis of the HTNs and HTNs-NH<sub>2</sub>

HTNs were prepared by a previously reported template hydrothermal method [22]. In order to obtain uniformly sized HTNs, SiO<sub>2</sub> templates were prepared by the modified Stöber method in an innovative route. Then TiO<sub>2</sub> shell with a certain thickness was deposited on the SiO<sub>2</sub> template via a sol-gel procedure to obtain SiO<sub>2</sub>@TiO<sub>2</sub>. Then, the core/shell material was calcined at 800°C for 1.5 h to achieve the expected crystal phase. Finally, the SiO<sub>2</sub> cores were etched off with NaOH solution in an autoclave. Then the HTNs product was centrifuged, washed three times with ultra pure water and dried at powder at 60°C. The structure and morphology of the synthesized HTNs was characterized by SEM and TEM images as shown in Fig. 1. We could see that the size dimension of HTNs by this

method ranging from 100 to 140 nm, and the main size of inner diameter about 80 nm, and the shell thickness only about 20 nm (inset in Fig. 1A). It expressed that the cavity was full enough for electron to be reflexed and refracted multiply, so that the electron cloud density was deepened in the conjugate structure of luminol and copolymer, thus the electrical signal was increased many times.

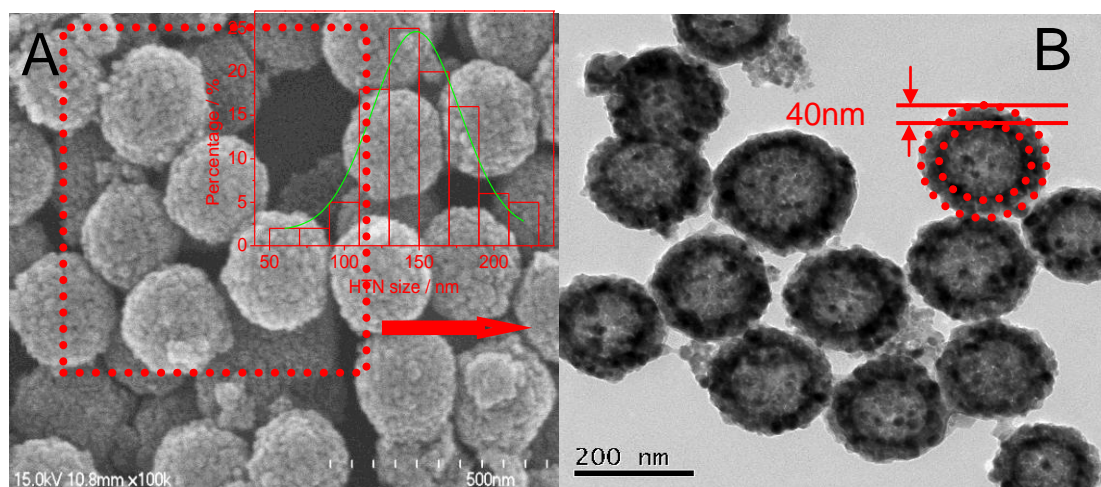


**Figure 1.** The SEM (A) and TEM (B) of HTNs. The inset in (A) shows the particle-size distribution histogram. The red dots in (B) indicate corresponding thickness of nano - shell HTNs.

Then the -NH<sub>2</sub> grafted HTNs was fabricated in mixture solution at room temperature as reported [23]. Typically, 50 mg of HTNs was suspended in the solution of 50 mL ethanol and 5 mL H<sub>2</sub>O. After sonicated for 10 min and magnetic stirred for 30min, 0.05 mL APTES was transferred into the mixture, then the reaction was carried out for 8 h under magnetic stirring. After the suspension was boiling in water bath for 30min, cooling and being static for a while, the -NH<sub>2</sub> grafted HTNs (HTNs-NH<sub>2</sub>), was centrifuged and washed with absolute ethanol to remove any unreacted chemicals.

#### 2.4. Preparation of HTNs-PLA/ITO and other electrodes

Before modifying, pieces of ITO glass (cut into 1 cm × 5 cm sheets) were washed in sequence with ultra pure water, ethanol : 1 mol/L NaOH (1:1, v / v), diluted ammonia and ultra pure water for 15min each time in an ultrasonic bath and then dried with a nitrogen stream. Then the above ITO was used as the working electrode in a normal three-electrode system to carry out electro-polymerization from 0.0V to +1.0 V in stirred modified solution, which containing 0.5 M H<sub>2</sub>SO<sub>4</sub>, luminol and aniline (0.005 M and 0.01 M, respectively). Certainly, luminol and aniline were organic compounds with the low solubility in water solution. A new chemical category of ionic liquids (IL) for use as solvents and phase transfer catalyst have been used in many electrochemical applications because of their high ionic conductivity, biocompatibility and molecular viscosity [24]. Moreover, the appropriate selection of IL in polymerization can also improve the polymerization degree and productivity because of its participation as a monomer [25]. In this work, 1mg L<sup>-1</sup> of 1-ethyl-3-methylimidazolium chloride

(EMIL) was used as the IL addition prepared as the literature [26, 27]. The modified electrode was signed as HTNs-PLA/ITO. At the same time, the HTNs/PLA/ITO, PLA/ITO and PL/ITO electrodes were also prepared to compare the electrochemical properties.

### 2.5 Sample preparation and detection

Before detection of ACT residue in the strawberry under the optimum detection conditions, the extraction and pre - process of the sample was essential to obtain accurate measurement results and to avoid interference determination of complex components. The strawberry was chopped and weighed 20 g into a 250 mL Erlenmeyer flask containing 50 mL acetone. And then was ultrasonic extracted for two times after shaken for half an hour vigorously, with each extraction time for 5 min. The combined filtrate was then added into 50 mL mixture of ethanol and water (v% 1:1) and ultrasonicated for 5 min in the presence of 10 g sodium chloride. Then the solution was extracted with dichloromethane three times sequentially with partial 30mL. The combined dichloromethane extracts were then dried before concentration to dryness. Then the analyte was dissolved with 10 mL petroleum ether and subjected to SPME as reported [10]. Analytes were eluted with 5 mL solution of petroleum ether - acetic ether (95/5, v / v), and the eluate was concentrated to dryness. Then the residue was redissolved in dichloromethane (2 mL) for direct detection.

## 3. RESULTS AND DISCUSSION

### 3.1 Characterization

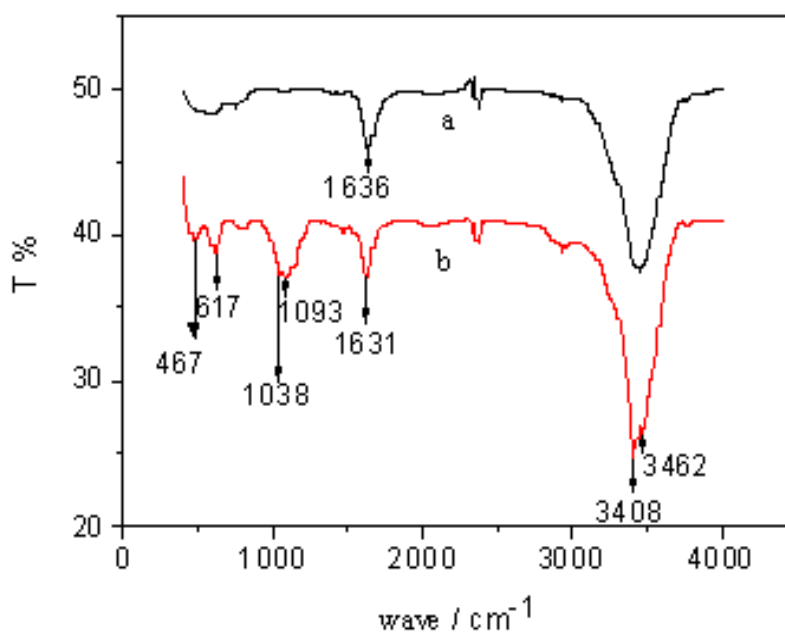


**Figure 2.** The FTIR of (a) HTNs and (b) HTNs-NH<sub>2</sub>.

The FTIR spectrum in Fig.2 was the comparisons of HTNs (a) and HTNs-NH<sub>2</sub> (b). Compared with curve a, the peak exceeding 3400 cm<sup>-1</sup> became sharp and was divided into two peaks at 3462 cm<sup>-1</sup> and 3408 cm<sup>-1</sup> in curve b, which identified the intramolecular and intermolecular hydrogen bonds in –NH<sub>2</sub>. The 1038 cm<sup>-1</sup> and 1093cm<sup>-1</sup> was the bending vibration peak of Si-O-Si in plane and out of plane, respectively. The absorption peak at 1636 cm<sup>-1</sup> (in curve a) was the typical characteristic peak of O-Ti-O, but it shifted blue about 5 cm<sup>-1</sup> (in curve b). The 467 cm<sup>-1</sup> and 617 cm<sup>-1</sup> was the stretching and bending vibration peak in the Ti-C-Si, respectively, showing that the APTES was grafted on the surface of HTNs.

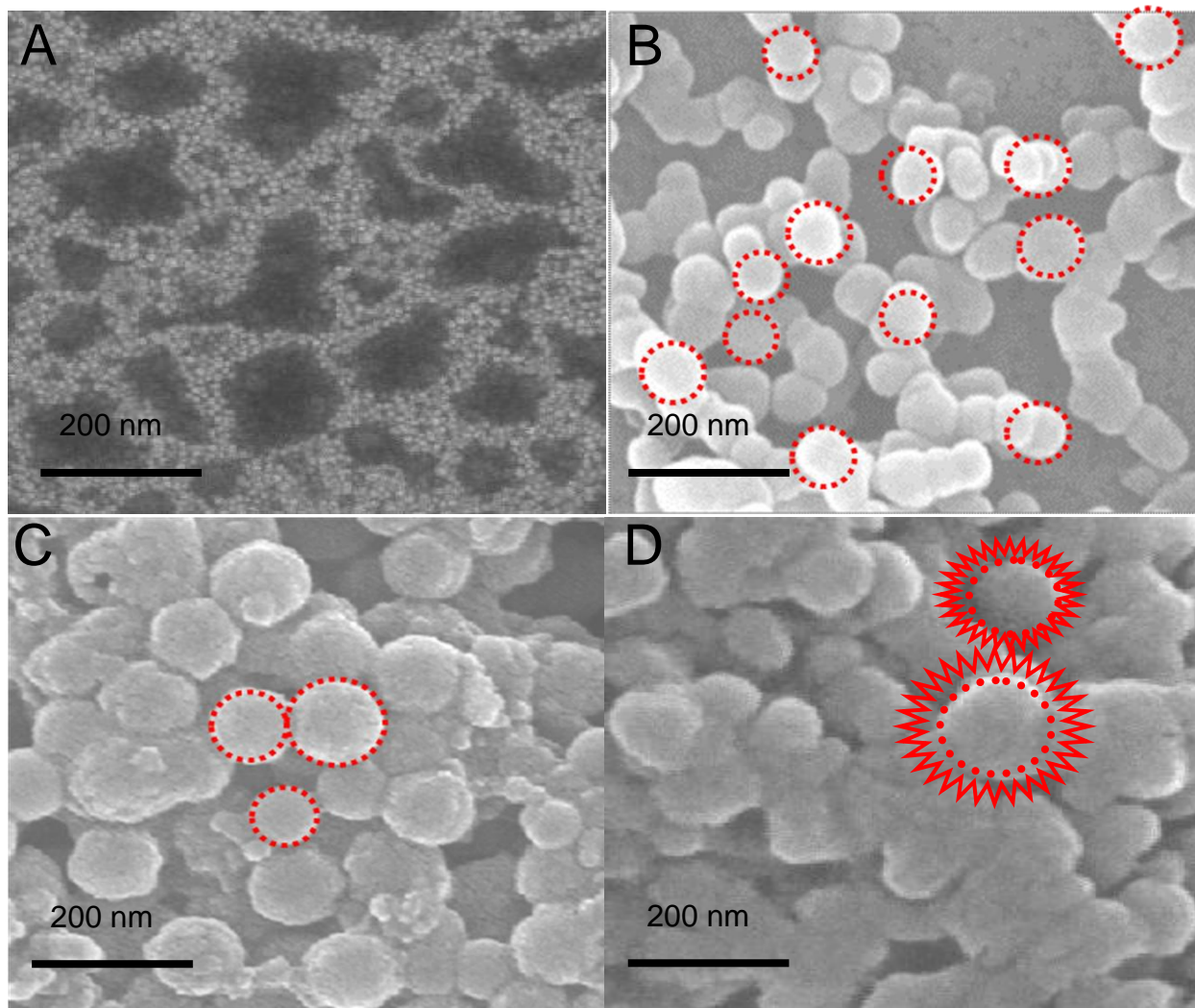


**Figure 3.** The SEM images of PLA (A), HTNs-PLA (B), HTNs / PLA / ITO(C) and HTNs @ PLA (D). The red dots in (B, C and D) indicate HTNs on the surface of electrode.

As descriptions of the polymerization mechanism [28, 29] between luminol and aniline, the polymerization reaction would occur through the linkage of –NH– with the para-carbon of the phenyl rings in an acidic medium. In Fig.3A, the SEM image of PLA presented network pattern. The soft skeleton of the para-carbon of the phenyl rings formed multiple structures, resulted in a densely

stacked porous sphere by crinkling or folding. The Fig.3B showed the morphology of the HTNs-PLA. Obviously, the HTNs could be seen clearly in the copolymer as circling in red. Moreover, the distribution trajectory of HTNs consisted with the PLA, which identified the participation of HTNs in the process of electro copolymerization. In addition, the size dimensions of HTNs were uniform just like electrical screening. This state benefited to form a homogeneous film. For the convenience of comparison about the morphology, the HTNs/PLA (the HTNs was dropped on the surface of PLA) and HTNs @ PLA (the HTNs was chemical oxidized with PLA) were displayed in Fig.3C and Fig.3D. Seen from the surface in Fig.3C, the HTNs of different size was tiled randomly and stacked relatively dense, and the shape of PLA pre - polymerization on ITO could not be visible at all. In Fig.3D the surface of HTNs @ PLA was rough. The diameter of HTNs became larger than bare HTNs, and the shape of HTNs was vague because it was wrapped in the hybrids copolymer. In comparison, the HTNs-PLA film seemed homogeneous and uniform.

### 3.2 Performance

Fig.4A presented the typical electrochemical impedance spectroscopy (EIS) to obtain the interfacial properties of the several electrodes. As we could see, the EIS of bare ITO (curve a), HTNs-PLA / ITO (curve b), PLA / ITO (curve c) and PL / ITO (curve d) was  $28\Omega$ ,  $50\Omega$ ,  $110\Omega$  and  $150\Omega$ , respectively. Although PL and PLA have the analogous linear skeleton of PANI for electron transfer, the PL polymer presented poor conductivity because of its more compact structure of lateral hydrazide groups [30]. Easily, when aniline units were inserted into the PLA, the charge transfer resistance (Rct) decreased, meaning that it had higher conductivity. And when HTNs participated in the copolymerization at the same time, the Rct of the HTNs-PLA / ITO decreased vastly meaning the more easily charge transfer resulted from the conjugation of the conductive HTNs in the copolymer.

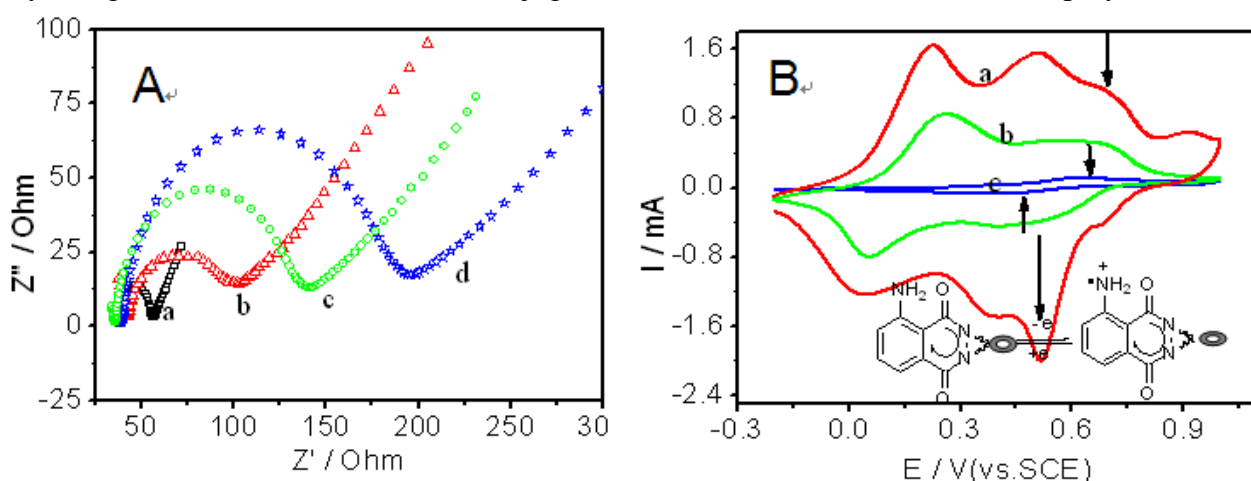


**Figure 4.** (A) The EIS of (a) bare ITO, (b) HTNs-PLA/ITO, (c) PLA/ITO and (d) PL/ITO in 0.1M NaCl supporting electrolyte solution containing 5mM  $[\text{Fe}(\text{CN})_6]^{3-/4-}$ . (B)The CVs of (a) HTNs-PLA/ITO, (b) PLA/ITO and (c) PL/ITO in 0.5 M  $\text{H}_2\text{SO}_4$  solution at a scan rate of  $50\text{mV s}^{-1}$ . Inset in (B) shows the redox process of HTNs conjugate in luminol structure.

The CVs of HTNs-PLA, PLA and PL in 0.5 M H<sub>2</sub>SO<sub>4</sub> could indicate the contribution of HTNs or aniline to the resulting polymer at the electro activity (Fig.4B). In the comparison between PLA and PL, because of low electro activity of PL (curve c), the well-defined redox couple 0.46/0.53V in curve b corresponded to the reversible redox of luminol at 0.43/0.59V in curve c, but the peak current improved 6 times. The other redox couple at 0.09/0.23V of leucoemeraldine / emeraldine attributed to copolymerization with aniline, resulted in an emerald green surface of electrode. The most interesting was that there were 4 redox couples in curve a; and all the couple peak currents presented at least 5 times growth compared to PLA (curve b). The new emerging couples at 0.53/0.65V and 0.70/0.83 became very obvious and symmetric, and they were attributed to the conversion of pernigraniline / emeraldine and emeraldine / leucoemeraldine, respectively [31]. Especially the peak current at 0.46/0.59V redox couple became very obvious and the reduction peak appeared very sharp, which was contributed to an increase of 8 times from luminol. In fact, the lateral hydrazide group (–CO–NH–NH–CO–) in the luminol structure presented poor conductivity. But after the copolymerization of HTNs in acid IL solution, its conductivity was enhanced more obviously than PLA. This appearance enlightened the discussion on the structure and formation process of the copolymer, which retained the basic skeleton structure of PLA.

### 3.3 Structure and mechanism

As reported, the hydrazide group in the structure of luminol was easy to hydrolyze under the acid condition and easy to be replaced or be introduced by the amino or amide group in other molecule [32]. In this polymerization system, at first, the HTNs-NH<sub>2</sub> replaced the diamine in the hydrazide group, which increased the electronic transfer ability and electron cloud density of acylhydrazine ring. Thus, the redox ability of luminol was increased heavily as inserted in the Fig.4B. Moreover, the clear and visible HTNs in the SEM (fig.3B) and the growth of all peak currents implied the participation of HTNs in the copolymerization. The ortho carbon position of the amino in the aromatic ring became an active site in the process of polymerization, and easily polymerized to be a new large conjugate aromatic ring, in order to reduce the position energy in the process of polymerization and increase the stability of the polymer [33]. So, secondly for the maximum stability, a new hexatomic ring on the basis of PLA was also formed easily by the conjugate of HTNs-NH<sub>2</sub> in the polymer. In fact, because of much more HTNs-NH<sub>2</sub> in the mixture, the electro - copolymerization reaction happened not only in the chain, also in the layer. In view of this, the copolymerization mechanism and fabrication process could be deduced as in Fig.5. The symmetrical shape kept the lowest energy and the highest stability, which looked like a symmetrical flower-like structure.

Thus, the arrangement mode of the HTNs-PLA could explain the above micromorphology and electrochemical phenomena. And the simulation structure of the HTNs-PLA was deduced too. The arrangement of the polymer and the replacement positions of HTNs in different colors were obviously expressed in Fig.5, which benefitted to the explanation on the increase of the stability and catalytic activity of copolymer.

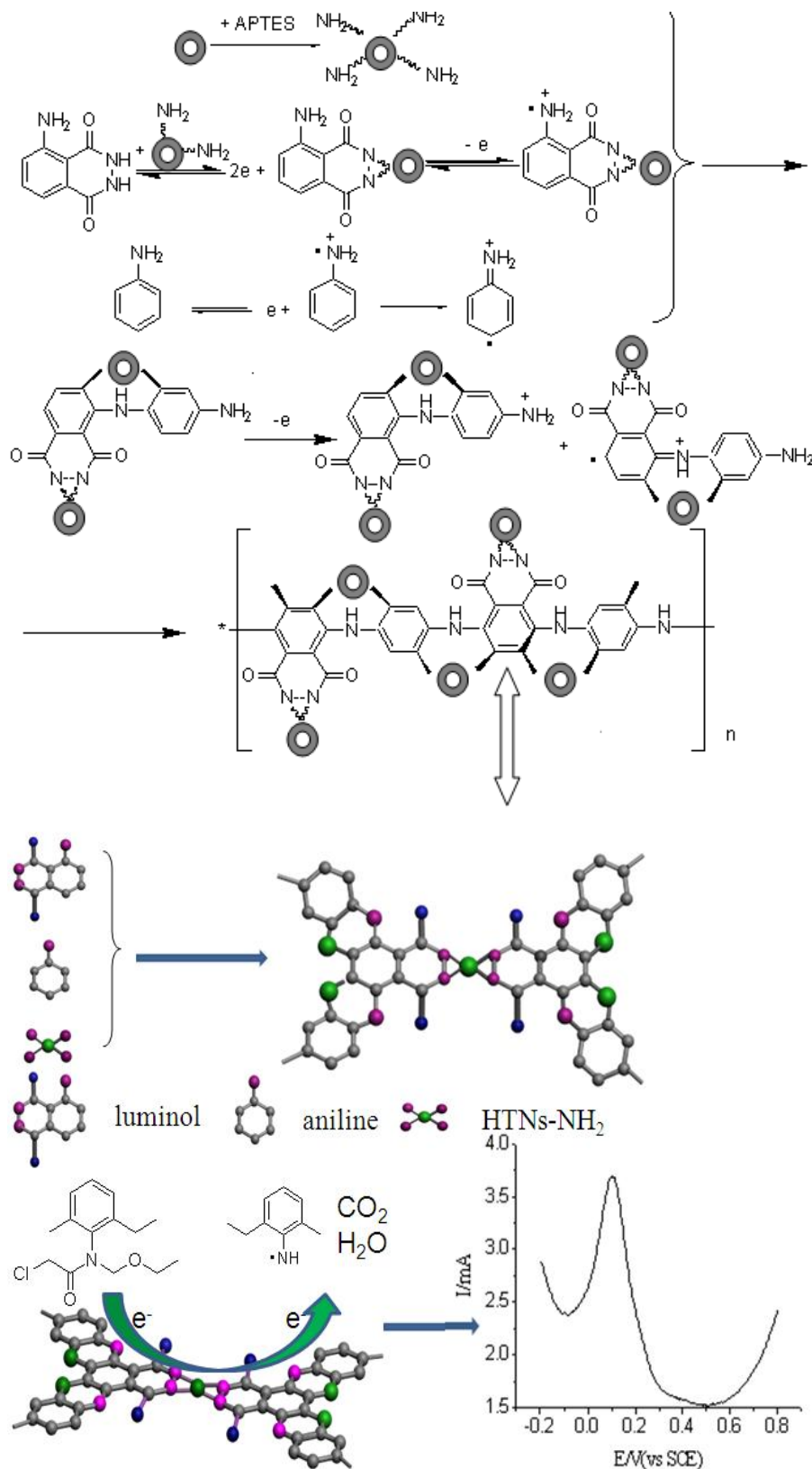


**Figure 5.** The formation mechanism of HTNs-PLA and schematic illustration of electrocatalytic process for ACT.

### 3.4 Optimization of the preparation

Because of the different molecular diffusivity, different molecular weight and size of luminol, aniline and HTNs, some important parameters such as scan rate and sample dosage should be optimized to obtain a stable and homogeneous electrocatalysis film. As shown in Fig.6A, when scan rate was selected at  $150 \text{ mV s}^{-1}$ , because of the longer chain and thicker film of PLA, the conjugation of HTNs in the new six ring became compact, and the arrangement of HTNs appeared to be irregular, resulted in an inhomogeneous film. Similarly when the scan rate dropped to  $50 \text{ mV s}^{-1}$ , the three dimension of copolymer became more obvious, but the skeleton of PLA film became softer under the slower scan rate causing some HTNs enclosed in porous PLA (Fig.6B) resulted in a rough surface of copolymer, which was inhomogeneous too. Overall consideration of the homogeneity and stability, the scan rate in the process of electro-polymerization was selected at  $100 \text{ mV s}^{-1}$ .

The dosage of aniline in polymerization was also optimized. As anticipated, with the concentration of aniline increasing from 0 to 0.01M, the electron transport capability improved regularly. As known, the pivotal structure of PANI would enhance the electron transfer ability, but the excessive ratio of aniline to luminol made the polymer film became denser, and the copolymerization of HTNs was also influenced. So the aniline concentration in the stirred mixture was controlled at 0.01M in the next experiment.

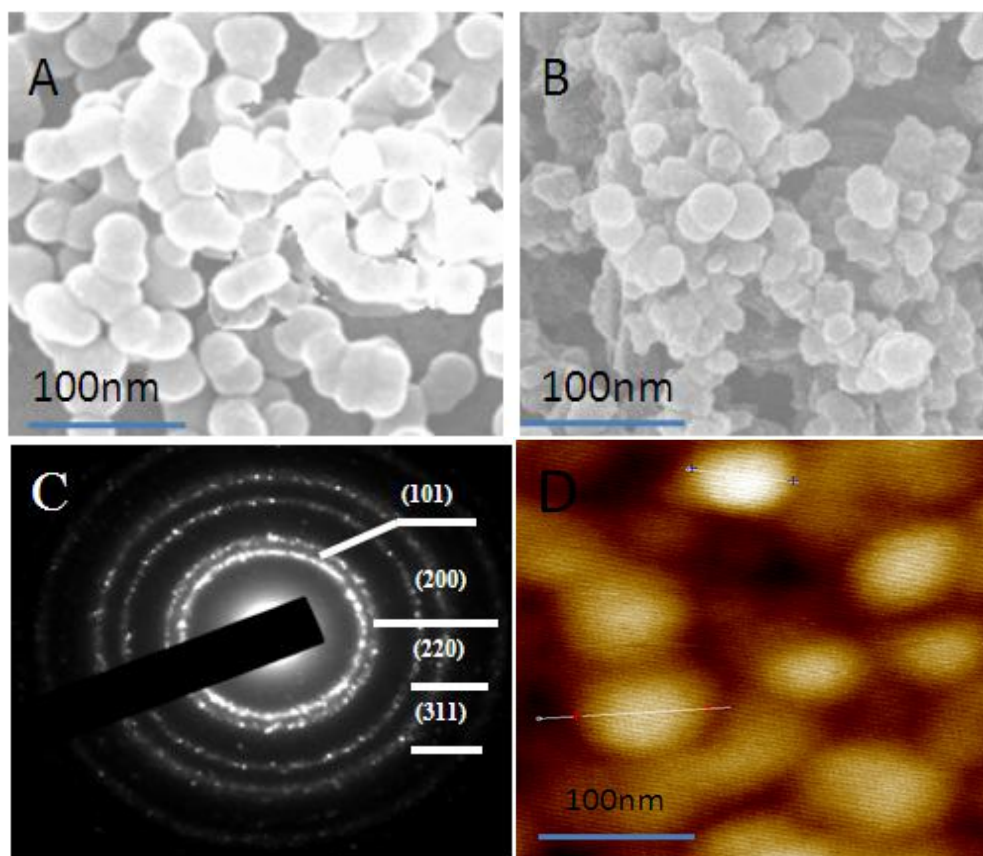


**Figure 6.** The SEM image of HTNs-PLA/ITO at different scan rate  $150 \text{ mV S}^{-1}$ (A) and  $50 \text{ mV S}^{-1}$  (B). The SAED pattern (C) and AFM image (D) of HTNs-PLA.

After the above optimization, the crystalline nature of HTNs-PLA was characterized by SAED. The several distinct rings indicated the polycrystalline structure of HTNs-PLA [34], demonstrating the ordered arrangement of HTNs in the copolymer, which were not enwrapped in the PLA. And typically, some spots could be observed in these rings (Fig.6C), implying more HTNs in the conjugate polymer and some HTNs on lattice point retained partial properties of single crystals [35]. At the same time, the morphology of HTNs was captured by AFM method shown in Fig.6D. The bright circular substances were HTNs and its ordered arrangement in the polymer could be seen obviously, which testified the copolymerization mechanism in Fig.5.

### 3.5 Electrochemical properties and mechanism

Different electrocatalysis copolymer may produce different catalytic peak voltage and current for ACT on the modified HTNs-PLA/ITO, HTNs/PLA/ITO, PLA/ITO and PL/ITO. Fig.7A showed the comparison of 0.01mM ACT directly catalyzed on the above electrodes. The peak current of ACT on HTNs-PLA/ITO (curve a) was about 40 times than on PL/ITO (curve d), and much higher than on PLA/ITO (curve c) or HTNs/PLA/ITO (curve b). Moreover, the peak potential of ACT on HTNs-PLA/ITO presented the lowest at about 0.1V (vs.SCE). The other three electrodes catalyzed ACT exceeding 0.2V. As known, the linkage of phenyl ring was the basic skeleton whether in PL or PLA copolymer. The rigid active sites of  $\pi$  electron cloud and the hydrogen bond of  $-N-H\cdots N-$  was connected with the dense PL or PLA copolymer; but in the homogeneous film of HTNs-PLA, because of the rich electron density and the more active sites in the conjugate aromatic ring, the film of HTNs-PLA could become a nucleophilic reagent to the benzene in the structure of ACT, and weakened the bond energy of  $-CO-N-$  and  $-C-O-C-$ , which benefited to the hydrolysis, then the electrocatalysis reaction of the hydrolysate from ACT became much easier. So the electrocatalysis potential on HTNs-PLA film was the lowest.

The electrocatalysis mechanism of ACT on the film was simulated in Fig.5 too. In fact, the more nucleophilic actions in HTNs-PLA film and the more hydrogen bonds between HTNs-PLA and ACT were profitable to the hydrolysis effect. According to the report [36, 37], some organic small molecule alcohols and acids could be electrocatalyzed to form carbon dioxide and water on the nano - scale alloy with high electrocatalytic properties, which were the clean and harmless final products of carbon and hydrogen. Thus, in this proposed film, some hydrolysates from ACT on the surface were quickly catalyzed, and the electrical signal was recorded immediately. The electrocatalytic properties of HTNs-PLA were well adapted for the catalytic reaction of organic molecules.

### 3.6 Optimization of the detection

Because of the lack of electrochemical active group in the structure of ACT, it expresses the nonelectroactivity in the neutral condition. But as well known, in different acidic conditions, the  $-CO-NH-$  amide group can hydrolyze, which resulted in the change of the structure of ACT. So the pH value was the most important parameter in detection of ACT. Fig.7B showed the comparison of

0.01mM ACT on HTNs-PLA/ITO in the different pH value by DPV method. Obviously, when ACT was detected in the pH=7.0 phosphate condition, the peak current (curve a) was highest. When pH=6.5, or 6.0 (curve b and c), many ACT has already happened hydrolysis in the acid condition before detection, and the hydrolysates diffused rapidly in the phosphate solution. Thus the concentration of ACT on the surface of this proposed sensor decreased, which led to a decline of the current. And as the pH value increased to 7.5 or 8.0 (curve d and e), the peak current of ACT on HTNs-PLA/ITO was even lower than the item in pH value 6.5 or 6.0. In fact, the acidity of copolymer on the surface of sensor would also decline in alkaline condition, resulted from the neutralization reaction. And some copolymer may change its own structure leading to the loss of catalytic activity, so the electrocatalysis was affected and the peak current of ACT dropped down. Therefore, the optimum detection pH value was chosen at 7.0. Moreover the ideal remedy was that the catalytic copolymer would renovate after scanning for 5 cycles in the 0.5 M H<sub>2</sub>SO<sub>4</sub> solution between two detections. Then the 4 couples of transformation among emeraldine, pernigraniline and leucoemeraldine appeared again and the peak currents were the same as before.

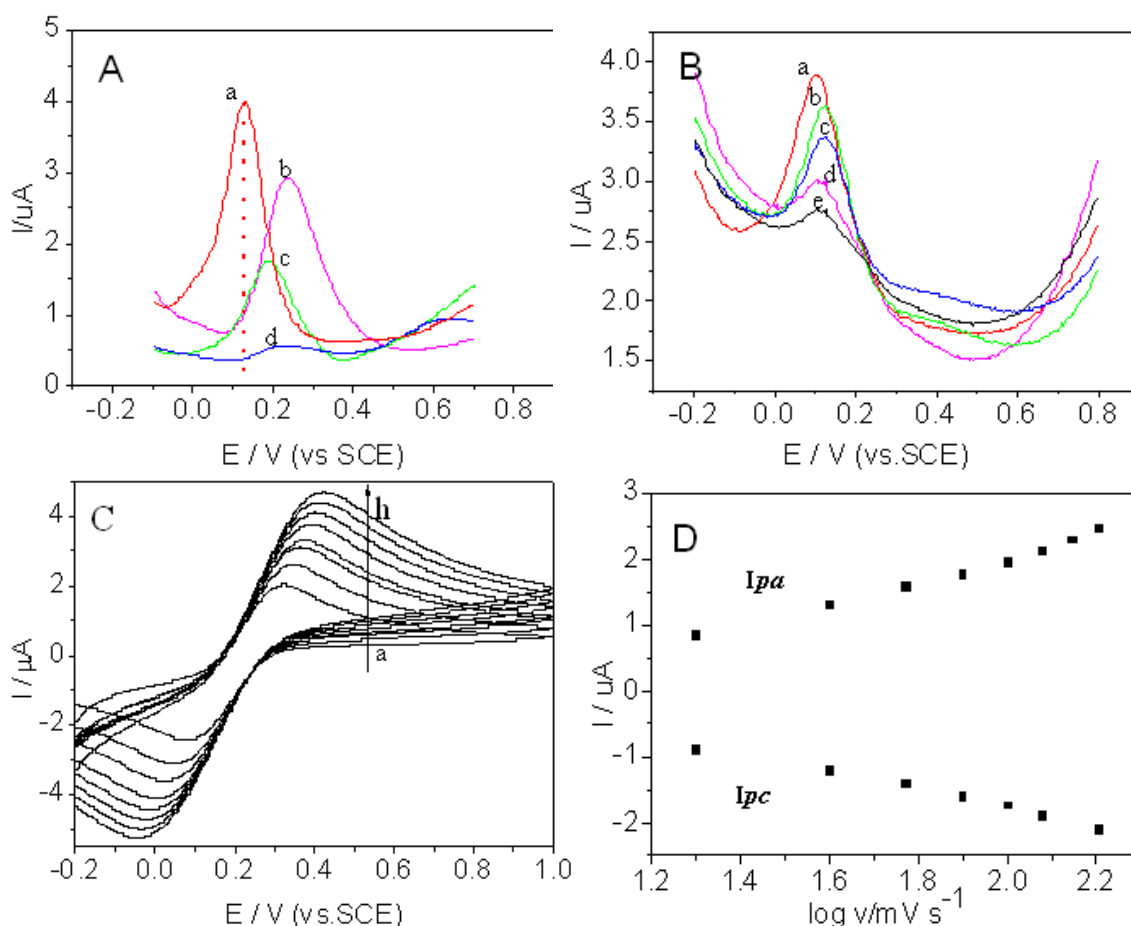


**Figure 7.** The DPV curves of 0.01mM ACT (A) on different biosensor (a) HTNs-PLA/ITO; (b) HTNs/PLA/ITO, (c) PLA/ITO and (d) PL/ITO; (B) in different pH values (Insert: the CVs of ACT); (a)7.0; (b) 6.5 and (c) 7.5; Pulse amplitude: 50mV; pulse width: 50ms; pulse period: 200ms. (C) The CVs of HTNs-PLA/ITO at different scan rates, (a)-(h): 20, 40, 60, 80, 100, 120, 140, 160  $\text{mVs}^{-1}$ . (D) The relationship of cathodic / anodic peak current vs scan rate.

The effect of scan rates in the detection process on the voltammetric behavior was monitored using 5mM  $\text{Fe}(\text{CN})_6^{3-/4-}$  (0.1M KCl) as the probe shown in Fig.7C. The redox potentials of the electron transfer at HTNs-PLA/ITO showed dependence on scan rate. The anodic and cathodic peak potentials shifted to positive and negative directions, respectively. And the peak current showed good linear dependence on  $\log V$  in the range of 20-160 mV/s (from a to h) as in Fig.7D, indicating the occurrence of surface confined the process at the electrode. This was accordance with the report [38]. And the detection result depended mostly on the concentration of ACT on the surface of the electrocatalysis sensor. The influence from scan rate consisted with the effect from the acidity of the phosphate solution. So the scan rate was important and the 100 mV/s value was optimum.

### 3.7 Detection performance

Under optimized conditions, the ACT proposed sensor exhibited a linear response within the concentration ranging from  $2.0 \times 10^{-7}$  M to  $1.5 \times 10^{-5}$  M, and an absolute detection limit of  $0.15 \times 10^{-9}$  M at a signal-to-noise ratio of 3. The linear concentration was shown in Fig.8A. Compared to the indirect detection methods such as PB, FPI and PEB sensors, this proposed sensor with a symmetric flower-like structure had higher stability, sensitivity and lower detection limit. Because of the synergistic effect between the two components among HTNs, aniline and luminol, and their original perfect catalytic activity, the electro-copolymer film of HTNs-PLA had better electrocatalytic activity. So the linear range was wider than LC and GC methods as listed in Table 1. The detection optimum pH value was kept in 7.0 instead of acid or alkaline condition, which made the ACT molecule retain itself structure and reacted under the sensor's catalysis. The detection concentration was the direct amount of ACT in the tested solution. Although its detection limit was higher than that using GC-MS ( $10 \text{ ng L}^{-1}$ ), the proposed method still conformed to the environmental measurement standards regulated by the UDEPA (the maximum residue limits in ground sample,  $0.1 \mu\text{g L}^{-1}$ ). Moreover, this proposed sensor was easily and quickly fabricated, having good electrocatalytic performance. In fact, the electrocatalytic activity would benefit the application of this proposed sensor for the determination of the oxidizable and reducible residue in the environment.

**Table 1.** Analytical performances of different methods for ACT detection

method	Linear range	Detection limit	Optimum pH	Reference
HPLC-MS	$0.27\text{-}0.44 \mu\text{g kg}^{-1}$	$0.2 \mu\text{g kg}^{-1}$	-	[8]
GC-MS	$10.0\text{-}250.0 \text{ ng L}^{-1}$	$10 \text{ ng L}^{-1}$	-	[39]
GC-ECD	$0.01\text{-}1.0 \mu\text{g mL}^{-1}$	$0.01 \mu\text{g mL}^{-1}$	-	[10]
PB	$0.2\text{-}100.0 \mu\text{g L}^{-1}$	$0.2 \mu\text{g L}^{-1}$	11.0	[12]
FPI	$0.01\text{-}10.0 \mu\text{g mL}^{-1}$	$10 \text{ ng mL}^{-1}$	8.0	[13]
PEB	$5.4\text{-}13.5 \mu\text{g mL}^{-1}$	$0.054 \text{ ng mL}^{-1}$	9.0	[14]
Proposed sensor	$0.054\text{-}4.05 \mu\text{g mL}^{-1}$	$40.5 \text{ ng L}^{-1}$	7.0	This work

After pre-processing of the two strawberry samples purchased from Local orchard, the redissolved solution in dichloromethane (described in the preceding paragraph 2.5) was used to directly determine ACT residues. Fig.8B showed the DPV scanning curves of original extraction (curve a) and added 0.001mM ACT in it (curve b) using the same electrochemical sensor, scanning for 5 cycles in the 0.5 M H<sub>2</sub>SO<sub>4</sub> between two intervals in the detection of the sample. Obviously, the peak marked by arrow was the electro catalytic signal of ACT. The detection and recovery results of the added ACT sample for three times were found to be accordance very well with those obtained by conventional GC-MS method as listed in Table 2.

Certainly, a 0.01mM ACT solution was measured by 5 HTNs-PLA/ITO electrodes prepared as the same method, and the RSD of this detection method was 2.8%, implying the excellent reproducibility. After using 5 times and stored for one week in refrigerator at 4°C, the detection results were accordance with original signal by the renovated electrocatalysis sensor.

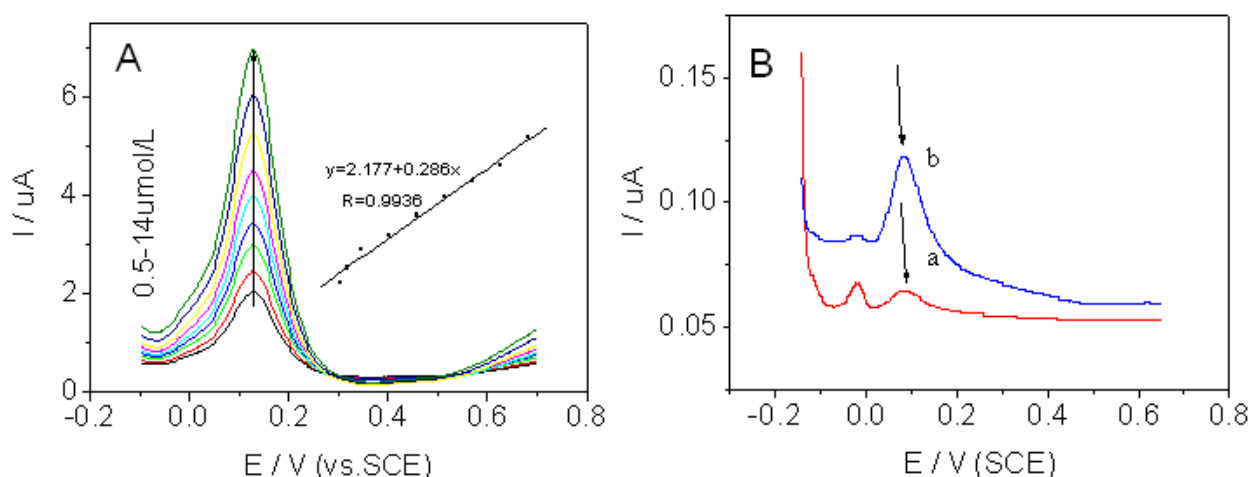


**Figure 8.** (A) The DPV curves of ACT detection at different concentrations. Inset was the linear equation of peak current vs concentration. (B) The DPV curves of original strawberry extraction (curve a) and added 0.001mM ACT in it (curve b); other conditions as in Fig.7A and B.

**Table 2** Detection results and recoveries of ACT in strawberry

sample	This sensor (μM)	GC-MS (μM)	Added (μM)	Found (μM)	Recovery (%)	RSD (%)
#1	0.78	0.80	1	1.38	91.6	2.78
	0.75	0.77	5	5.57	88.7	2.34
	0.77	0.78	10	10.46	90.5	3.01
#2	0.53	0.55	1	1.43	93.5	2.28
	0.51	0.53	5	5.38	91.3	2.89
	0.54	0.56	10	10.29	92.7	3.25

Because ACT was the main component to control of grasses in strawberry, Other ingredients were separated in the pretreatment process of strawberry sample by SPME, so in order to obtain

accurate detection results, it was important for sample pretreatment method. But the interferences from nutrient soil, some inorganic ions such as  $\text{NH}_4^+$ ,  $\text{K}^+$ ,  $\text{Na}^+$ ,  $\text{Ca}^{2+}$ ,  $\text{Mg}^{2+}$ ,  $\text{Al}^{3+}$ ,  $\text{SO}_4^{2-}$ ,  $\text{NO}_3^-$ , organic compounds urea and ascorbic acid were also investigated. They had no influence on the detection of ACT residue in strawberry. These results implied that this proposed method was practical for real sample detection.

#### 4. CONCLUSIONS

A simple electrochemical method was designed for the nonelectroactive ACT detection. The catalytic film with a novel homogeneous and symmetric flower-like structure was easily and quickly fabricated. The ordered symmetric arrangement of HTNs made the copolymer keep the polycrystalline nature, and especially promoted the electron transfer ability of acylhydrazine in luminol structure. The proposed electrocatalysis sensor presented the good stability, low detection limit. Especially, its reproducibility was very perfect after scanning for 5 cycles in 0.5 M  $\text{H}_2\text{SO}_4$  solution. After optimization of copolymer film and detection parameters, it was used to electro catalyze and detect ACT residues in strawberry, and the detection results were well accordance with that using GC-MS method.

#### ACKNOWLEDGEMENT

This work was financially supported by the Jiangsu Natural Science Foundation of China (13KJB150035) and Agricultural Infrastructure Project of Suzhou Science and Technology Development Plan (Grant No. SYN201507).

#### References

1. C. Xu, W.Q. Tu, M. Deng, Y.X. Jin, B. Lu, C.N. Zhang, C.M. Lin, Y.M. Wu and W.P. Liu, *Chemosphere*, 164(2016) 618.
2. M.E. Foley, V. Sigler and C.L. Gruden, *ISME J.*, 2(2008) 56.
3. T. Zerin, H.Y. Song and Y.S. Kim, *Toxicol. in Vitro*, 29 (2015) 85.
4. X. Cai, G. Sheng and W. Liu, *Chemosphere*, 66 (2007) 286.
5. Y. Li, Q. Chen, C.H. Wang, S. Cai, J. He, X. Huang and S.P. Li, *Bioresour. Technol.*, 148 (2013) 628.
6. J.H. Jiang, S.G. Wu, X.J. Liu, Y.H. Wang, X.H. An, L.M. Cai and X.P. Zhao, *Environ. Toxicol. Pharmacol.*, 40 (2015) 516.
7. T.T. Dagnac, F. brgm, R. Jeannot, C. Mouvet and N. Baran, *J. Chromatogr., A*, 957 (2002) 69.
8. Y.G. Li, Z.L. Chen, R. Zhang, P. Luo, Y. Zhou, S. Wen and M.H. Ma, *Chromatographia*, 79 (2016) 1165.
9. S. Yasmine, B. Stéphane, B. Sophie, O.K. Kresten, S. Michel and R.A. Henrik, *Sci. Total Environ.*, 458–460(2013) 527.
10. J.Y. Hu, Z.H. Zhen and Z.B. Deng, *Bull. Environ. Contam. Toxicol.*, 86(2011) 95.
11. J. Yakovleva, A.V. Zherdev, V.A. Popova, S.A. Eremin and B.B. Dzantiev, *Anal. Chim. Acta*, 491 (2003) 1.
12. Y.L. Mikhail, A.E. Sergei and S. Petr, *Anal. Lett.*, 36 (2003) 2443.
13. M.A. Deryabina, Y.N. Yakovleva, V.A. Popova and S.A. Eremin, *J. Anal. Chem.*, 60 (2005) 80.

14. D.Q. Jin, Q. Xu, Y.J. Wang and X.Y. Hu, *Talanta*, 127 (2014) 169.
15. D.Q. Jin, A.Q. Gong and H. Zhou, *RSC Adv.*, 71(2017) 17489.
16. S. Xie, K. Ouyang, Y.M. Lao, P.H. He and Q. Wang, *J. Colloid Interface Sci.*, 493 (2017) 198.
17. S. Tang, Q. Zhao and Y.F. Tu, *Sens. Actuators, B*, 237 (2016) 416.
18. G.X. Li, J. Lian, X.W. Zheng and J. Cao, *Biosens. Bioelectron.*, 26 (2010) 643.
19. V. Ferreira, A.C. Cascalheira and L.M. Abrantes, *Electrochim. Acta*, 53 (2008) 3803.
20. C.B. Xiao, Q. Zhao and Y.F. Tu, *Electrochim. Acta*, 147 (2014) 791.
21. C.Liu, X.H.Wei and Y.F.Tu, *Talanta*, 111 (2013)156.
22. H.L. Shen, H.H. Hu, D.Y. Liang, H.L.Meng, P.G. Li, W.H. Tang and C. Cui, *J. Alloys Compd.*, 542 (2012) 32.
23. H.N. Cao, J. He, L. Deng and X.Q. Gao, *Appl. Surf. Sci.*, 255 (2009) 7974.
24. N. Maleki, A. Safavi and F. Tajabadi, *Anal. Chem.*, 78 (2006) 3820.
25. R.C. And and L.F. Vega, *J. Phys. Chem. B*, 110 (2006) 14426.
26. P.Y. Chen and I.W. Sun, *Electrochim. Acta*, 46 (2001) 1169.
27. J.K. Chang, S.Y. Chen, W.T. Tsai, M.J. Deng and I.W. Sun, *Electrochem. Commun.*, 9 (2007) 1602.
28. Y.J. Wang, G.X. Li and X.W. Zhen, *Chinese J. Anal. Chem.*, 53 (2008) 3803.
29. G.F. Zhang and H.Y. Chen, *Anal. Chim. Acta*, 419 (2000) 25.
30. B. Jugović, M. Gvozdenović, J. Stevanović, T. Trišović and B. Grgur, *Mater. Chem. Phys.*, 114 (2009) 939.
31. A. Elsanousi, E.M. Elssfah, J. Zhang, J. Lin, H.S. Song and C. Tang, *J. Phys. Chem. C*, 111 (2007) 14353.
32. S. Muna and S.J. Cho, *Anal. Chim. Acta*, 688 (2011) 70.
33. M.J. Bojdys, J. O. Müller, M. Antonietti and A. Thomas, *Chem. Eur. J.*, 14 (2008) 8177.
34. P. Santhosh, K.M. Manesh, A. Gopalan and K.P. Lee, *Anal. Chim. Acta*, 575 (2006) 32.
35. D. Kusum and C.S. Pundir, *Enzyme Microb. Technol.*, 96 (2017) 177.
36. D.N. Li, A.J. W, J. Wei, Q.L. Zhang and J.J. Feng, *J. Colloid Interface Sci.*, 514(2018) 93.
37. L.X. Chen, L. Liu, J.J. Feng, Z.G. Wang and A.J. Wang, *J. Power Sources*, 302 (2016) 140.
38. S. Ribbens, V. Meynen, G.V. Tendeloo, X. Ke, M. Mertens, B.U.W. Maes, P. Cool and E.F. Vansant, *Microporous Mesoporous Mater.*, 114 (2008) 401.
39. D. P. Capel, Ma. Lin, R.S. Blaine, J. S. Larson and A.G. Therese, *Environ. Sci. Technol.*, 29(1995)1702.